

Map Space Belief Prediction for Manipulation-Enhanced Mapping

Joao Marcos Correia Marques^{1*} Nils Dengler^{2,3,4*} Tobias Zaenker^{2,5} Jesper Mücke²
 Shenlong Wang¹ Maren Bennewitz^{2,3,4} Kris Hauser¹

* These authors contributed equally to this work

1. University of Illinois at Urbana-Champaign, IL, USA 2. Humanoid Robots Lab, University of Bonn, Germany
 3. The Lamarr Institute, Bonn, Germany 4. The Center for Robotics, University of Bonn, Germany

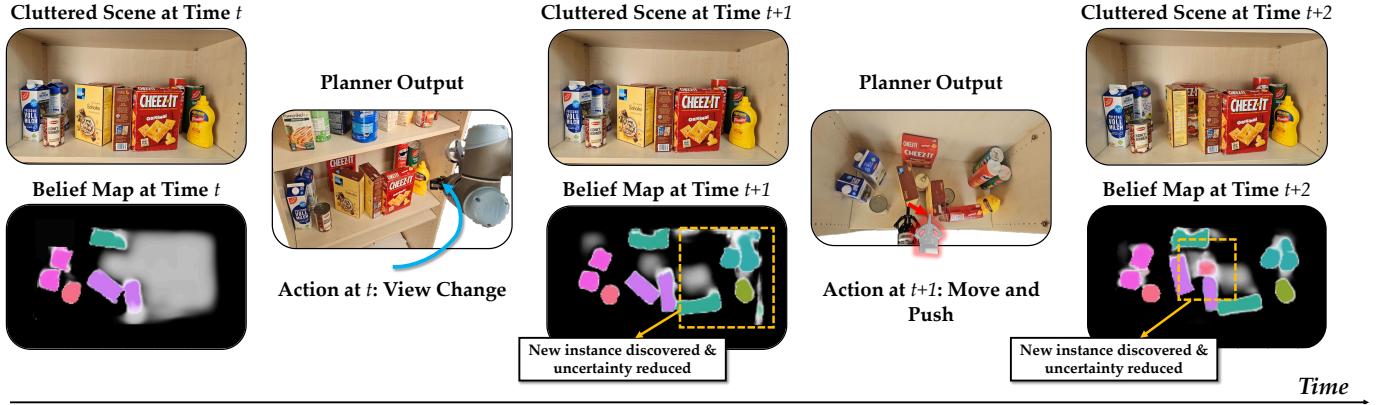


Fig. 1: Example scenario with occlusions in a confined shelf environment. Given a current partial map of the environment (belief t), our planner decides whether gathering another observation or manipulating the scene would be best to reduce map uncertainty. In this example, first a viewpoint action would increase environmental knowledge, followed by a push to unveil the hidden can behind the two boxes at time $t + 2$.

Abstract—Searching for objects in cluttered environments requires selecting efficient viewpoints and manipulation actions to remove occlusions and reduce uncertainty in object locations, shapes, and categories. In this work, we address the problem of manipulation-enhanced semantic mapping, where a robot has to efficiently identify all objects in a cluttered shelf. Although Partially Observable Markov Decision Processes (POMDPs) are standard for decision-making under uncertainty, representing unstructured interactive worlds remains challenging in this formalism. To tackle this, we define a POMDP whose belief is summarized by a metric-semantic grid map and propose a novel framework that uses neural networks to perform map-space belief updates to reason efficiently and simultaneously about object geometries, locations, categories, occlusions, and manipulation physics. Further, to enable accurate information gain analysis, the learned belief updates should maintain calibrated estimates of uncertainty. Therefore, we propose Calibrated Neural-Accelerated Belief Updates (CNABUs) to learn a belief propagation model that generalizes to novel scenarios and provides confidence-calibrated predictions for unknown areas. Our experiments show that our novel POMDP planner improves map completeness and accuracy over existing methods in challenging simulations and successfully transfers to real-world cluttered shelves in zero-shot fashion.

I. INTRODUCTION

Active sensing has long been studied in robotics for tasks such as exploring an unknown environment [1], complete 3D object model acquisition [24], and searching for an unobserved target object [28, 14, 49]. To build complete maps as efficiently as possible, Next Best View (NBV) planning [48] is often employed to reduce the uncertainty about the map as quickly

as possible. Although NBV planning offers an approach for static scenes in which the robot simply moves the camera passively through free space, there are many applications, such as household and warehouse robotics, in which robots may need to manipulate the environment in order to gain better viewpoints [13, 34]. We refer to this problem as *manipulation-enhanced mapping* (MEM). MEM offers two significant new challenges beyond standard NBV problems. First, in order to decide when and where to manipulate objects, the robot should reason about how object movement may affect previously occluded regions. Second, it must anticipate the impact of manipulations on observed objects and possibly partially-observed or unobserved objects. For example, pushing boxes in a grocery shelf backward will move them simultaneously until the furthest, occluded box hits a wall.

MEM is related to the *mechanical search* problem [11] in which the robot manipulates clutter to reveal a target object. Prior approaches in mechanical search tend to rely on restrictive assumptions, such as a static viewpoint, which ignores a robot’s ability to look around obstacles [20, 41]. Other studies assume full observability of object dynamics and poses [38] or are limited to a fixed set of predefined objects [46]. These assumptions are too limiting for complex cluttered scenes like shelves. The most closely-related work to ours is Dengler et al. [13] who address these limitations by training a reinforcement learning policy for viewpoint planning and learn a heuristic manipulation policy. However, the heuristic nature of this approach can lead to inefficient performance,

as waiting for information gain saturation to push gathers many viewpoints around minutiae that could be more quickly revealed by manipulation.

This paper formulates the MEM problem as a Partially Observable Markov Decision Process (POMDP) in the belief space of semantic maps. By maintaining map-space beliefs, our approach is applicable to unstructured cluttered environments with an arbitrary numbers of objects. The POMDP computes the next best viewpoint or manipulation action that maximizes the agent’s expected information gain over a short horizon (Fig. 1). Our approach leverages neural network methods for map-space belief propagation, which have been shown in the object goal navigation literature to drastically improve map completion rates and offer better guidance for object search [14, 49]. The key challenge in belief propagation with manipulation actions is that they often reduce certainty when the object’s dynamics are unknown or the robot interacts with unobserved objects. To address this challenge, we introduce the Calibrated Neural-Accelerated Belief Update (CNABU) technique to learn unified belief propagation models for both viewpoint and manipulation actions. Confidence calibration is especially important for belief propagation because overconfidence in either object dynamics or map prediction can result in ineffective exploration and/or early termination. We employ evidential deep learning to do so [39].

Experiments show in simulation environments that our MEM planner outperforms prior work [13] and CNABU-enhanced baselines in terms of metric-semantic accuracy. Furthermore, we perform hardware experiments with a UR5 robot equipped with a gripper and an in-hand camera, demonstrating the zero-shot transfer of the learned models, and showing the efficacy of our method in mapping of cluttered shelves. **An implementation of our method will be made available on GitHub upon acceptance.**

II. RELATED WORK

A. Next Best Viewpoint Planning

NBV planning is a well-researched approach in the area of active vision that has been applied to both object reconstruction and large-scale scene mapping. Generally, NBV consists of two steps: First sampling view candidates, then evaluating which candidate is the best. For object reconstruction tasks like [19], views are usually sampled from a fixed set around the object. For large-scale scenes, sampling is more challenging. Monica and Aleotti [32] sample at the contour of the explored scene. Other approaches sample at either predefined or dynamically detected regions of interest. For the evaluation, most approaches compute an estimated information gain to determine the utility of a view. The information gain can be based on the expected entropy reduction, e.g. by counting unknown voxels in the field of view. Other approaches like Hepp et al. [18] rely on a learned utility to predict the best view. In this work, we build upon existing concepts of NBV planning, but enhance them by incorporating manipulation actions to interactively shape and explore the environment,

allowing the robot to gather richer information and adapt its strategy based on both observation and interaction.

B. Mechanical Search in Shelves and Piles

Mechanical search algorithms [11, 20, 40] locate and extract one or multiple target objects from a given scene, while dealing with confined spaces, occlusion and object occurrence correlations. The task consists of multiple steps, i.e., visual reasoning, motion and action planning as well as their precise execution. For visual reasoning, current research demonstrates that the scene can be effectively explored by interacting with objects [3, 13, 28, 34] to actively reduce or overcome occlusions, but most works consider a fixed viewpoint [20, 11, 40].

Kim et al. [23] propose a method for locating and retrieving a target object using both pushing and pick-and-place actions. However, their approach relies on a fixed camera, lacks a long-term map, and rebuilds environmental knowledge from scratch with each observation. Therefore, the approach can lead to unnecessary manipulation actions, as the target may already be visible from other viewpoints. In the context of planning for manipulation among movable objects (MAMO) [37, 42], Saxena and Likhachev [38] introduced a method for object retrieval in cluttered, confined spaces. Despite achieving strong retrieval performance, their approach depends entirely on prior knowledge of object shapes and dynamics. In this work, we do not focus on retrieving desired objects, but on mapping the constrained environments containing them. With our long-term occupancy and semantic map representation, retrieval plans can be generated without relying on perfect model knowledge or single-shot scene understanding.

C. Learned World Dynamics Models

Many model-based reinforcement learning algorithms try to learn environment models from episodic environmental interaction, often in latent spaces for evaluation speed, like Dreamer [16]. These models, however, do not result in a human-interpretable representation like our learned map-space dynamics. Recently, with the popularity of conditional video diffusion models, interactive “pixel-space” simulators have been developed, like UniSim [47] and [45]. These models, however, focus on visual fidelity, ignoring the uncertainty calibration in their representation and long-term temporal consistency often needed for robotics tasks provided by maps.

III. PROBLEM DEFINITION

We address the MEM problem as follows: Consider an environment with a set of movable objects of varying sizes and orientations, where some objects may be occluded and not directly observable from any viewpoint. The arrangement of these objects, along with the fixed support geometry (e.g., a shelf or table), constitute the workspace configuration space C^w [6]. Initially, the environment is assumed to be in an initial configuration $c_0 \in C^w$.

The robot’s objective is to create an accurate representation of the workspace configuration c_t after the execution of a sequence ζ of actions $[a_0, \dots, a_n]$. These actions include two

types: **viewpoint actions** where the robot moves its camera to a specific viewpoint $v_t \in \mathcal{V}$ to capture an RGB-D image, and **manipulation actions**, where the robot interacts with the scene (e.g., pushing or grasping). We address the eye-in-hand RGB-D camera setting in which the robot does not receive informative observations during manipulation and must instead move to a retracted viewpoint to receive valid depth data due to minimum depth restrictions. Moreover, we do not integrate views during movement between locations, since such images are subject to motion blur.

To formalize the problem, let the robot's internal representation of the environment, a factorized belief in the form of a metric-semantic map, be denoted as Φ_t . When the robot executes a manipulation action a_t , it causes a transition from $c_t \mapsto c_{t+1} \in \mathcal{C}^w$ according to the environment's dynamics $c_{t+1} = \text{Dyn}(c_t, a_t)$. Additionally, whenever the robot takes any action a_t and gets an observation o_t drawn according to the observation function $Z(o_t | a_t, c_t)$, its internal representation is updated through the belief update function $\Phi_{t+1} = \text{BelUpdate}(\Phi_t, a_t, o_t)$.

Finally, similar to Choudhury et al. [8], we define MEM as an optimal budgeted mapping problem. The robot is given a maximum action budget T , and an initial environment configuration c_0 , which is *a priori* unknown. The task is to output the most informative sequence of actions ζ such that the robot's internal map belief Φ_T , at the last step of the budget, maximizes its mean Intersection over Union (mIoU) to the ground truth map Φ_T^{GT} which represents c_T . So we have:

$$\begin{aligned} \zeta^* &= \arg \max_{\zeta=[a_0, \dots, a_{T-1}]} \text{mIoU}(\Phi_T, \Phi_T^{GT}) \\ \text{s.t. } \Phi_T^{GT} &= \text{GroundTruth}(c_t) \\ c_{t+1} &= \text{Dyn}(c_t, a_t) \forall t \\ \Phi_{t+1} &= \text{BelUpdate}(\Phi_t | a_t, o_t), o_t \sim Z(c_t | a_t, c_t), \forall t \end{aligned} \quad (1)$$

where $\text{BelUpdate}(\cdot)$ represents the robot's belief update, $Z(\cdot)$ the observation function, and $\text{GroundTruth}(\cdot)$ an “oracle” that yields the map that would be built if the robot had perfect knowledge of the environment. In deployment, the robot does not have access to such an oracle or the dynamics of the environment.

IV. METHOD

A. Overview

We model the OBM problem as a Partially Observable Markov Decision Process (POMDP) in map-space, with the following parameters: $\{S, A, T, R, Z, O\}$. The state $s \in S$ comprises the robot's configuration $q_t \in \mathbb{R}^{D_{\text{DoF}}}$, where DoF is the number of Degrees of Freedom of the robot, assumed to be fully observable, and the workspace configuration that is partially observable through semantically labeled RGB-D observations. The ground truth configuration c_t is represented by a metric-semantic map in the form of a dense voxel grid $\Phi_t^{GT} \in \mathbb{N}^{H \times W \times D}$ with height H , width W , depth D , and M classes. Thus, state s at time t is defined as (q_t, Φ_t^{GT}) . The transition function $T : \mathcal{C}^w \mapsto \mathcal{C}^w$ encodes the object dynamics in the scene and is *a priori* unknown. Furthermore,

the action space A consists of two types of actions: viewpoint actions ($a \in A^v$) and manipulation actions ($a \in A^m$). Viewpoint actions modify only the fully observable robot state and generate a partial observation $o \in O$, as defined by the observation function Z . In contrast, manipulation actions alter the workspace configuration but do not provide any observations of the environment. The reward function $R(t)$ is approximated using the Volumetric Information Gain (VIG) metric [12], as directly modeling the mIoU metric is not feasible, as it depends on the inaccessible ground truth.

To solve this POMDP, the agent must perform an accurate belief update about the state of the map, after both manipulation and observation actions. However, the high dimensionality of the space of all possible maps makes traditional POMDP belief updates computationally infeasible [22]. A common approximation of this belief update is to consider that the map's cells are all independent, as commonly done in occupancy grid mapping [43]. However, this leads to an imprecise representation of the belief, as it fails to incorporate known priors about the world, like object contiguity and usual object sizes and arrangements in its update. To address this, we propose leveraging uncertainty-aware deep learning models to predict a factorized belief distribution that is better aligned with plausible map configurations, while retaining the compactness of the factorized belief representation of independent cells.

B. Deriving Factorized Belief Dynamics

To propose an effective method for training these networks, we first outline the conditions required for an ideal factorized belief update within the map space. Consider an RGB-D image with added semantics as observation $o_t \in O$, taken from a camera fixed to the robot's end-effector. Following grid mapping literature [43], we represent our belief Φ_t of the environmental state as a dense $H \times W \times D$ voxel grid of independent cells, $m_t^{i,j,k} \in M$, each tracking their own occupancy probability. Additionally, we use an $H \times W \times N_{\text{classes}}$ 2D birds-eye semantic map of independent cells $sm_t^{i,j}$, where N_{classes} is the total number of a closed set of semantic classes. In the following, we focus on occupancy beliefs, but the beliefs over the semantic states follow a similar reasoning.

Our formulation implies that the belief assigned to any state s is given by Eq. 2, where $s^{i,j,k}$ denotes the occupancy state of a cell with coordinates (i, j, k) .

$$b(s) = \prod_{m_{i,j,k} \in M} P(m^{i,j,k} = s^{i,j,k}) \quad (2)$$

Suppose that there exists a function $\Omega(\Phi_t, s) = P(s | \Phi_t)$ that accurately computes the probability of any state s given the current belief Φ_t , action a_t , observation o_t , and $Z(o_t | s, a_t)$ as observation model. Then, the POMDP belief update equation [22] is given by:

$$P_t(s) = \frac{1}{\eta} Z(o_t | s, a_t) \sum_{s' \in \mathcal{C}^w} T(s | a_t, s') \Omega(\Phi_{t-1}, s'), \quad (3)$$

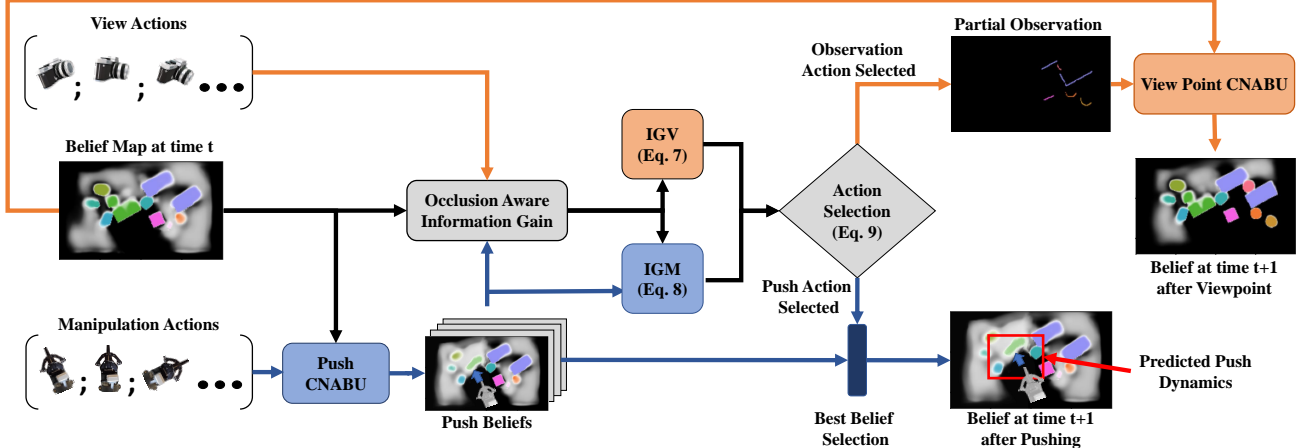


Fig. 2: From a prior map belief, our pipeline predicts the potential map belief resulting from a series of potential pushes. It then weighs the information gain from taking two consecutive independent views given the current belief (orange arrows) or taking a single observation given any of the predicted beliefs after pushing (blue arrows), selecting the path of highest cumulative information gain and taking its respective first action - either taking the next best view or executing the best push.

where s' is any other possible state and $P_t(s)$ indicates the probability of state s at time t , with η being a normalizing constant. Given these probabilities, the marginalized occupancy probability of any element $m_t^{i,j,k} \in \Phi_t$ is defined as

$$P(m_t^{i,j,k} = 1) = \mathbb{E}_{s \sim P_t(s)} [\mathbb{I}_{s^{i,j,k}=1}], \quad (4)$$

where $\mathbb{I}_{(\cdot)}$ is the indicator function and \mathbb{E} is the expected value. For semantic mapping this can be described using a naive average or histogram-based update of the semantics [9].

C. Approximating Belief Dynamics with Neural Networks

According to our problem definition, viewpoint actions will never cause a transition on the non-observable part of the state. Therefore, whenever a new viewpoint action is performed, Eq. 4 reduces to:

$$P(m_t^{i,j,k} = 1) = \frac{1}{\eta} \sum_{s' \in S} z(o_t | s, a_t) \Omega(\Phi_{t-1}, s) \mathbb{I}_{s^{i,j,k}=1} \quad (5)$$

Our method recursively estimates this update using a deep posterior network [44], $\sigma_o(\Phi_{t-1}, o_t)$, which we call Calibrated-Neural Accelerated Belief Update (CNABU) network. Since any scene that could produce a belief Φ_t via its observations is inherently a sample of the distribution induced by this belief, we leverage a neural network's averaging tendency to create an implicit Monte-Carlo estimate of Eq. 5 by recursively estimating $\Phi_t = \sigma_o(\Phi_{t-1}, o_t)$ from prior Φ_0 .

However, when using a manipulation action, no new observation is generated, but the action leads to a transition in the scene. Therefore, Eq. 4 simplifies to:

$$P(m_t^{i,j,k} = 1) = \frac{1}{\eta} \sum_{s' \in S} T(s | a_t, s') \Omega(\Phi_{t-1}, s) \mathbb{I}_{s^{i,j,k}=1} \quad (6)$$

Since this update does not depend on any observations, we propose to learn it through an action specific manipulation CNABU, $\sigma_m(\Phi_{t-1}, a_t)$. For improved flow, we delay the description of the training of these networks to Sec. IV-G and Sec. IV-H and proceed with describing how to use these trained

CNABUs to solve map-space POMDPs for unstructured interactive environments. Onwards, for brevity, we denote factorized occupancy and semantic belief representations (maps) by $\Phi_t = (\Phi_t^O, \Phi_t^S)$, respectively.

D. Solving the POMDP

We propose to solve the map-space POMDP by using a k -step receding horizon greedy planner, as shown in Fig. 2, which uses Volumetric Information Gain (VIG) [12] as an approximation of the true reward. VIG correlates to information gain and is a submodular optimization objective in static scenes [25], having been used to efficiently solve NBV planning and sensor placement problems. Due to VIG's submodularity, a greedy policy for solving this problem leads to bounded suboptimality, justifying the greedy receding-horizon strategy. While VIG's submodularity does not hold in general for a dynamic scene representation, we assume that manipulation actions are rare enough so that the submodularity assumption is still true for the majority of the policy execution.

Due to the submodularity of our objective, the greedy search horizon k can be short. However, because a manipulation action does not produce any observation, thereby offering no immediate information gain, at least one observation must be considered after a manipulation action. This requirement establishes the minimum search horizon at $k = 2$. For computational efficiency, we set our considered horizon to its minimum value.

To perform an observation action, the robot chooses from $v^i \in \mathbb{V}$ possible views in a fixed array of camera positions \mathbb{V} to which the robot can move. Furthermore, let $\theta_t \in \Theta_t$ be a sampled manipulation action from a set of feasible actions. In our two-step greedy search, we only consider two possible kinds of action sequences: taking two observation actions (v_t, v_{t+1}) or performing a manipulation action followed by an observation (θ_t, v_{t+1}) . This is, because (θ_t, θ_{t+1}) would result in no observation and therefore no information gain and

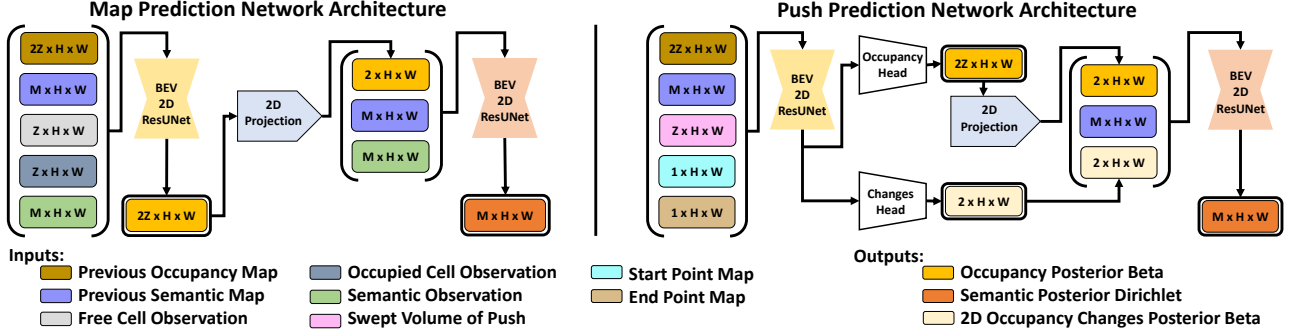


Fig. 3: Architecture overview of our observation and manipulation CNABU networks. The observation prediction network uses the occupancy posterior beta and semantic posterior Dirichlet for loss computation, while the manipulation prediction network additionally takes the 2D map of occupancy changes after the push for loss calculations.

the information gain of (v_t, θ_{t+1}) is strictly smaller than the VIG by any $(v_t, v_{t+1}), v_{t+1} \neq v_t$.

Given that $IG(v^i, \dots, v_{i+n-1} | \Phi^O)$ yields the Volumetric Occlusion-aware Information Gain [12] for voxels intersected by the rays from n views $(v^i \dots v^{i+n-1})$ given belief Φ^O , the two most informative consecutive views (v_t^*, v_{t+1}^*) , are:

$$(v_t^*, v_{t+1}^*) = \arg \max_{v_t, v_{t+1} \in \mathbb{V}} IG(v_t, v_{t+1} | \Phi_t^O) \quad (7)$$

For manipulation, $\tilde{\Phi}_{t+1}^{\theta_t} = \sigma_m(\Phi_t, \theta_t)$ denotes the predicted belief from the manipulation CNABU when given action $\theta_t \in \Theta_t$ as input. We can define the most informative 1-step push, θ_t^* and its associated most informative view $v_{\theta_t}^*$, as:

$$(\theta_t^*, v_{\theta_t}^*) = \arg \max_{\theta_t \in \Theta_t, v_{t+1} \in \mathbb{V}} IG(v_{t+1} | \tilde{\Phi}_{t+1}^{\theta_t}) \quad (8)$$

Finally, let $H(\cdot)$ represent the entropy of a given semantic map, with the entropy change defined as $\Delta H(\Phi_t, \Phi_{t+1}) = H(\Phi_t) - H(\Phi_{t+1})$. The term $IGV_t = IG(v_t^*, v_{t+1}^* | \Phi_t^O)$ denotes the best information gain obtained from two viewpoints, also called **viewpoint planning** (VPP), while $IGM_t = IG(v_{\theta_t}^* | \tilde{\Phi}_{t+1}^{\theta_t})$ represents the best information gain from a push followed by a viewpoint, which we will call **push selection**. Lastly, $Reg_t = \Delta H(\Phi_t, \tilde{\Phi}_{t+1}^{\theta_t})$ captures the entropy difference between the current semantic map and the map after the best push.

Our policy decides the action a_t to take according to:

$$a_t = \begin{cases} v_t^* & \text{if } IGV_t > IGM_t + \gamma Reg_t \\ \theta_t^* & \text{otherwise} \end{cases} \quad (9)$$

Where γ is a discount factor to account for different magnitudes between camera array VIGs and whole-map semantic entropy values. Reg_t serves as a regularization on the aggressiveness of the selected pushes, as more radical environment manipulations could potentially reveal more of the environment, but would cause unnecessary disturbances to the scene and introduce a lot more uncertainty to the post-push representations. If $a_t = \theta_t^*$, no observation is taken and $\Phi_{t+1} = \tilde{\Phi}_{\theta_t^*, t+1}$. If a_t is an observation action, we

get the observation o_t and use σ_o to obtain the new belief $\Phi_{t+1} = \sigma_o(\Phi_t, o_t)$. This search is then repeated in a loop until the maximum number of actions has been performed, or a threshold for full map completion has been reached, which we set to 95% of the semantic voxels with greater than 85% certainty in the belief Φ . When this threshold is reached, the planner no longer pushes, but still collects novel views.

E. Push Sampling

Our manipulation action of choice is pushing. To compute valid push candidates using Φ_t^O , we first compute the high-confidence frontier points from the shelf entry and sample k of them uniformly at random as start points for the pushes. We test the start points of the k sampled pushes for collisions against other high confidence voxels in Φ_t^O . For each valid start point, we sample a likely occupied point in Φ_t^O near it to obtain the push direction and sample a push distance uniformly at random between 50 and 150 mm. We then obtain a valid motion plan for the entire trajectory using a sampling based motion planner [15, 17] and use it to calculate an approximation of the robot's swept volume within the voxel map of interest and its start and end points encoded in 2D binary masks, which are the action parametrization inputs used in σ_m (Start Point and End Point maps in Fig. 3).

F. Dataset Generation

To train the CNABU models σ_o and σ_m , we collect datasets on maps, viewpoints, and sampled pushes in simulation. In order to sample realistic object configurations, a total of 14 different object categories from the YCB dataset [5] are used and sampled in a shelf board of size $(0.8 \times 0.4 \times 0.4)m$. We sample object configurations on the shelf following a stochastic method that considers class dependencies and efficient free space coverage for placing. This method allows for the sampling of varied object configurations, numbers and classes and is described in more detail in Appendix A.

To train the viewpoint belief prediction model σ_o , we assemble a dataset $\mathcal{D} = \{d_1, d_2, \dots\}$ where each d_i has the form $(m_{gt}, o_1, \dots, o_n)$. Here, m_{gt} represents the ground truth 3D metric-semantic voxel map of a shelf environment with randomly placed objects, and o_1, \dots, o_n are the depth

and semantic segmented images captured from V , the set of discrete viewpoints in the environment. The ground truth semantic labels are used in the rendered images.

To train the manipulation belief prediction model σ_m , the simulated robot executes a randomly sampled action in synthesized scenes. This produces a dataset $\mathbb{D}^a = \{d_1^a, d_2^a, \dots\}$ with each $d_i^a = (m_{gt}^{pre}, m_{gt}^{post}, o_1, o_2, \dots, o_n, \zeta)$, where $m_{gt}^{pre}, m_{gt}^{post}$ are the ground truth maps before and after manipulation, respectively, ζ is the parametrization of the executed action and o_1, \dots, o_n are observations as before.

G. Training the Viewpoint CNABU Network

We now detail the procedure for training the two CNABUs used in this work. Details of the architectures and features will be described in Appendix B. An overview of our network architectures is shown in Fig. 3. In this work, we presume that we have a closed-set of objects and a simulated environment on which we can place different numbers and arrangements of those objects.

Given that evidential posterior networks are shown to handle uncertainty more effectively [44], σ_o is designed to produce evidential outputs: $\alpha^S \in \mathbb{R}^{H \times W \times N_{classes}}$ and $\alpha^O \in \mathbb{R}^{H \times W \times D \times 2}$. These correspond to a grid of Dirichlet distribution parameters over a 2D map of the environment (with shape $H \times W$ and $N_{classes}$) and a dense 3D grid of Beta distribution parameters, one for each voxel in the environment (with shape $2 \times H \times W \times D$). Let $Dir(\cdot)$ and $Beta(\cdot)$ denote the Dirichlet and Beta distributions. Therefore, the semantic and occupancy beliefs used to solve the POMDP are defined as $\Phi^S = \mathbb{E}[Dir(\alpha^S)]$ and $\Phi^O = \mathbb{E}[Beta(\alpha^O)]$.

Given this dataset, we train σ_o by sampling, without replacement, a sequence of l posed depth and semantic images, $d' = (o'_0, \dots, o'_{l-1})$, from every d_i at every epoch. This sampling serves to encourage different beliefs to arise during training from the same scene with varying observation sequences. To avoid excessive indexing, we describe the training loop only for a single sequence d' .

We define α_t^S and α_t^O as beliefs computed via $\sigma_o(\alpha_{t-1}^S, \alpha_{t-1}^O, o'_{t-1})$, where the initial states α_0^S and α_0^O are uniform priors, represented as $\mathbb{1}$, a unit tensor with appropriate dimensions. Furthermore, we use y as a one-hot encoded tensor of the ground truth value for a given voxel. For the predicted distribution parameter $\alpha \in \alpha$, define $\tilde{\alpha} = y + (1 - y) \odot \alpha_i$, where \odot denotes element-wise multiplication. We employ the evidential uncertainty-aware cross-entropy from Sensoy et al. [39] to train this network with the following loss:

$$L_i^{type}(\alpha, y) = \mathcal{L}_i(\alpha, y) + \lambda KL(Dir(\tilde{\alpha}) || Dir(\mathbb{1})) \quad (10)$$

where $\mathcal{L}_i(\alpha, y) = \sum_{j=1}^M y_{ij} (\log(S) - \log(\alpha_{ij}))$, $KL(a || b)$ is the Kullback-Liebler divergence between distributions a and b , $\mathbb{1}$ is a vector of all ones, $type$ is o if it is an occupancy loss and s if it is a semantic loss and λ is an annealing parameter, set according to Sensoy et al. [39].

The total loss for the sample d' is the sum of the semantic and occupancy losses $L_i^o + L_i^s$ over l observations.

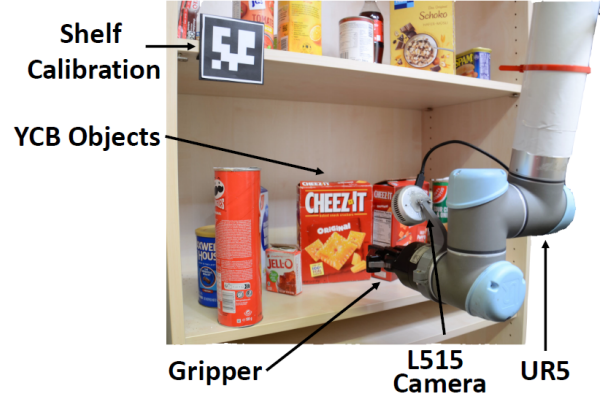


Fig. 4: Real-world environment showing a shelf scenario. The UR5 is equipped with an Robotiq parallel-jaw gripper and a Realsense L515 RGB-D camera to create a robust representation of the scene.

H. Training the Manipulation CNABU Network

The manipulation CNABU is defined similarly to the viewpoint CNABU, except it takes as an input the parametrization of action a_t , which we call ζ_t and it has an auxiliary output, which predicts a Beta distribution over a voxel grid modeling the probability of a given voxel being changed in Φ^{GT} after the manipulation is executed, which we call α^{diff} . Therefore, we have $\alpha_{t+1}^S \alpha_{t+1}^O, \alpha_{t+1}^{diff} = \sigma_m(\Phi_t, \zeta_t)$

To train σ_m , at each batch, we sample a sequence of $l \in [1, 10]$ images without replacement as above, and recursively obtain the beliefs from the σ_o CNABU, $\Phi_t = \sigma_o(\tilde{\Phi}_{t-1}, o'_t)$ and obtain $\alpha_{t+1}^S \alpha_{t+1}^O, \alpha_{t+1}^{diff} = \sigma_m(\Phi_t, \zeta_t)$. The random sampling of a different number of observations prior to pushing ensures the CNABU sees different belief stages during training. We derive the ground truth for α^{diff} , m_{gt}^{change} , from the difference between m_{gt}^{pre} and m_{gt}^{post} .

Finally, we add a fourth loss component, which we call consistency loss, L^{con} which is the Mean Squared Error between $(\alpha_{t+1}^S, \alpha_{t+1}^O)$ and (α_t^S, α_t^O) . This loss serves as a regularization to encourage the alpha parameters of the distributions in the unchanged areas of the map have a similar magnitude. As before, the network heads are trained using the loss in Eq. 10 [39]. So final loss for the manipulation CNABU σ_m is given by $L_i = L_i^O + L_i^S + L_i^{diff} + \epsilon L^{con}$.

V. EXPERIMENTS

We perform three experiments to evaluate our approach. First, simulation testing to highlight our pipeline's improvements in map completeness and accuracy, comparing it to S.O.T.A for manipulation-enhanced mapping by Dengler et al. [13]. Next, we present a series of ablations of our method and evaluate several interactive baselines. Finally, we study the robustness of our system in terms of its zero-shot transferability to a physical setup.

A. Experimental Setup

Our task setup consists of a shelf scene with a UR5 arm for observation and action execution. The robot is fixed to a table facing an occluded shelf and equipped with a Robotiq

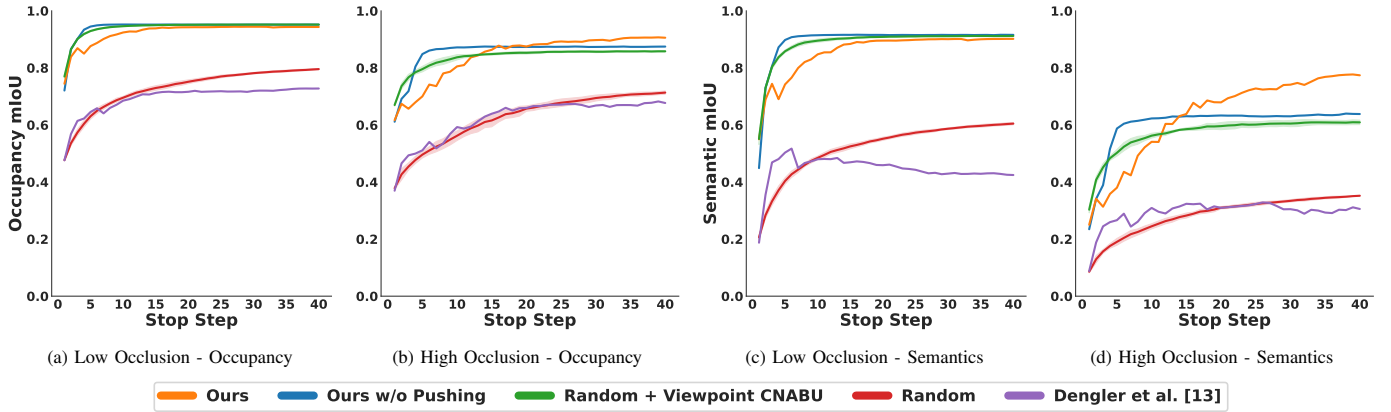


Fig. 5: Simulation results for Manipulation Enhanced Mapping against SOTA and non-pushing baselines- showing both occupancy and semantic IoUs over time for each method. Our method outperforms all baselines in highly occluded scenes, while not having degraded performance in low occlusion scenes. Standard deviation of performance of random baselines is represented as shading around each plot.

parallel-jaw gripper for manipulation and an RGB-D camera for observations. The Klamp’t library [17] is used for motion planning of observation and manipulation actions as well as swept maps as described in Sec. IV-E.

For the hardware experiments, we closely mimic the simulated scenario as shown in Fig. 4, with a few notable differences. For action execution, ROS and MoveIt [7] are used. The depth image is obtained from an intel Realsense L515 camera and the semantic segmentation in the real world is performed using segment anything 2 (SAM2) [36] and a strategy similar to LSeg [27, 21]. We take detected masks from SAM2 and crop the original image around them. Next, we extract their CLIP [35] embeddings and compute their cosine similarity to the language embeddings of our target classes, whose prompts we list in Appendix Sec. C. Finally, we normalize the similarity scores to classify each mask.

B. Simulation Experiments

Our simulation experiments consider both low and high occlusion scenarios for manipulation-enhanced mapping. We generate 100 low occlusion scenarios via rejection sampling, using our sampling method described in Appendix A, but keeping only scenarios for which at least one object cannot be seen from any of the 300 viewpoints. We then crafted 25 high occlusion scenarios by hand to be challengingly crowded and with many objects occluded. We provide examples of each in Figs. 9 and 10 in the appendix.

The robot always begins with a naive uniform prior over the environment. We measure the individual methods’ success in both metric and semantic mIoU against the ground truth map at time t , with a 40 step budget.

We compare our work against the following baselines. First, we re-implemented the approach by Dengler et al. [13], using the network weights provided by the authors, as their experimental setup closely matches ours. Second, the **Random** baseline randomly samples a set of unique views $[v_0^r, \dots, v_n^r] \in \mathbb{V}$ and employs standard metric-semantic occupancy mapping for map construction [43]. We also combine random view selection with our viewpoint belief predictor σ_o , **Random + Viewpoint CNABU**. These are compared against

our full pipeline with manipulation, **Ours**, and an ablation that eliminates manipulation, **Ours w/o pushing**.

Results are shown in Fig. 5. We observe that the previous S.O.T.A. for unstructured manipulation-enhanced mapping, Dengler et al. [13], is better than random sampling in the early steps, but performs worse than Random after more steps. We believe this happens due to heuristic action switching and lack of map prediction after pushing. Because it does not update its belief of the map after pushing, it takes several observations to reconcile the new scene with previously mapped regions, which it assumed were high certainly.

Moreover, we observe that belief prediction is a powerful approach, leading to excellent scene coverage in low occlusion scenes even without pushing. On highly occluded scenarios, pushing is required to make progress after the visible surfaces are observed. Our method uses pushing to achieve significant higher mIoUs. Note its IoU growth is slower early on, because pushing does not provide information until a viewpoint step is taken.

C. Push Selection Alternatives

Next, we validate our POMDP push selection strategy compared to other pushing strategies. In each compared strategy, we provide the same belief prediction networks as our method. Three of the strategies push regularly at a five step interval, which is the usual number of viewpoints before diminishing returns. The first, **Interval Random Pushing**, plans views using NBV and σ_o , and every 5 steps randomly samples a push and updates its belief using σ_m . The second, **Interval Random Pushing No Push CNABU** is the same, but does not use σ_m to update its belief after pushing. The third, **Random View Interval Random Pushing**, chooses random views and every 5 steps randomly pushes without using σ_m . Finally, we consider a heuristic that performs a random push when VIG seems to saturate, **Saturation Pushing**. The saturation threshold is when two consecutive estimates of VIG during NBV differ by less than 2%. Saturation pushing uses σ_m after each push to update its belief. A table of selection strategies shown in Sec. D in the Appendix.

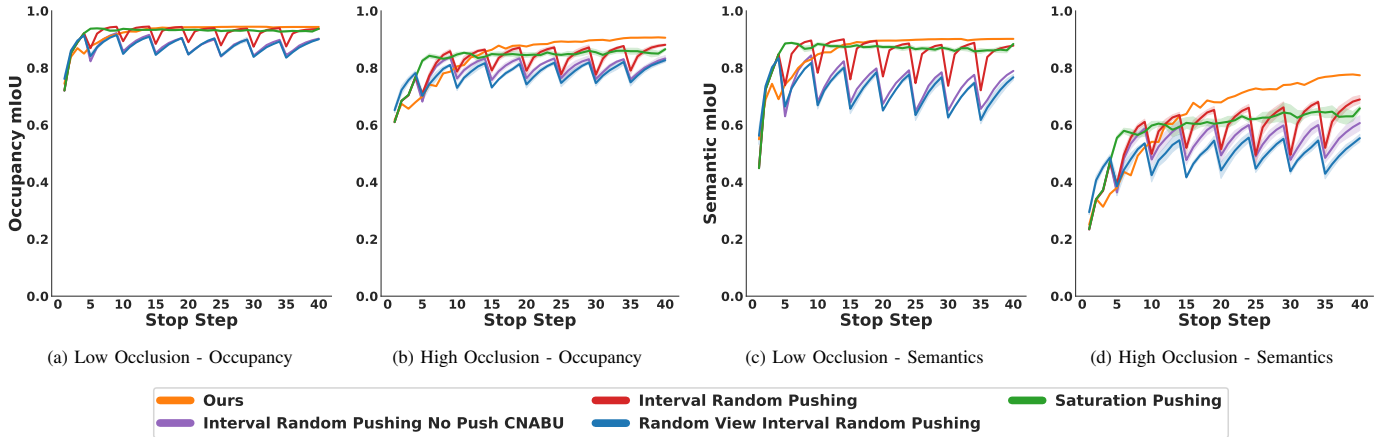


Fig. 6: Simulation tests of push selection alternatives. Note how our method not only achieves better mIoUs than any of the other methods, it does so consistently across all the steps, avoiding uninformative or overly aggressive manipulation actions. Also, next-best-view with the viewpoint belief prediction but without push belief prediction (purple) leads to degraded performance. Standard deviation of performance of random baselines is represented as shading around each plot

Results are shown in Fig. 6. Each baseline that has a random component is run three times with different random seeds. We observe that push belief prediction is beneficial to manipulation-enhanced mapping, even when random pushes are being executed. The blue and purple curves show methods that are not informed by σ_m . Further, we see that the saturation pushing (green) does not observe post-push performance drops, but it is ultimately outperformed by random informed pushes and our method. Overall, our method still achieves the best performance, most strikingly in highly occluded scenes.

D. Hardware Experiments

We also performed 10 real-world experimental runs on a UR5 as described in Sec. V-A. All results are collected in a zero-shot fashion, i.e., no fine-tuning on real data was performed. We set the budget to 20 steps and sampled a fixed set of 75 reachable camera poses in front of the shelf for \mathcal{V} .

We handcrafted 10 challenging scenes, each with an average of 18 objects from the YCB dataset [4], where pushing is required to reveal other objects. We collect the ground truths by removing the top of the shelf at the end of each episode to manually score the final maps. We score each scenario according to the status of **all of the objects** present in the map. Each object in the map is classified in four categories: 1) **Correctly Found** if the majority of the object is correctly represented in the map with the right class; 2) **Misclassified But Found** if the majority of the object is present in the occupancy map but is mislabeled; 3) **Not Found** - if the majority of the object is absent from the occupancy map and 4) **Hallucinated** if an object that is not present in the scene is present in the map. Due to the complexity of precisely resetting a scene multiple times for different baselines and the fact that both random + viewpoint CNABU and our approach without pushing are about as strong as other pushing baselines (see Figs. 5 and 6), we only compare against them in the physical experiments. For each model, we report the total quantity of each detection at time step 20 summed over all 10 trials.

Results in Tab. I show that with zero-shot transfer from sim-

to-real, the proposed method still manages to retain its edge over the compared baselines. Note that all methods compared use calibrated belief prediction. However, little difference is seen between viewpoint planning (Ours w/o Pushing) and random viewpoint choices. We expect that this is due to a domain gap caused by camera noise from the realsense L515 leading to some strong artifacting in the depth images and the inaccuracies of the open-set semantic segmentation pipeline. We found the SAM2 segmenter performed particularly poorly for oblique angles or partial object views, resulting in many missed instance detections and misclassifications. For instance, the segmentation pipeline persistently hallucinates a gelatin box as shown in the bottom right of the shelf, as seen in all methods in Fig. 7. Nevertheless, we can see that our methods (both with pushing and without pushing) greatly reduce the number of hallucinations and improve the number of correctly identified objects. Further, our complete pipeline reveals 39% of the objects that were previously unseen by the non-interactive baselines, performance consistent with the simulation experiments, despite the significant sim-to-real gap, particularly in segmentation performance, leading to many of the newfound objects being incorrectly classified.

TABLE I: Comparing our method to the strongest baselines in zero-shot transfer to real-world shelves. Total counts of each type of detection are reported across our 10 trials

Policy	Correctly Found \uparrow	Misclassified But Found \uparrow	Not Found \downarrow	Hallucinated \downarrow
Random	72	47	52	11
Ours w/o Pushing	81	38	52	6
Ours	85	52	35	7

VI. LIMITATIONS

Limitations of our method include the need for representative simulation training data or ground truth segmented maps. It also relies on high-quality semantic segmentation, and although the computer vision field is making significant progress on segmentation, segmentation accuracy is still too low for many robotics applications in occluded, poorly lit and partial views, especially in open-set scenarios.

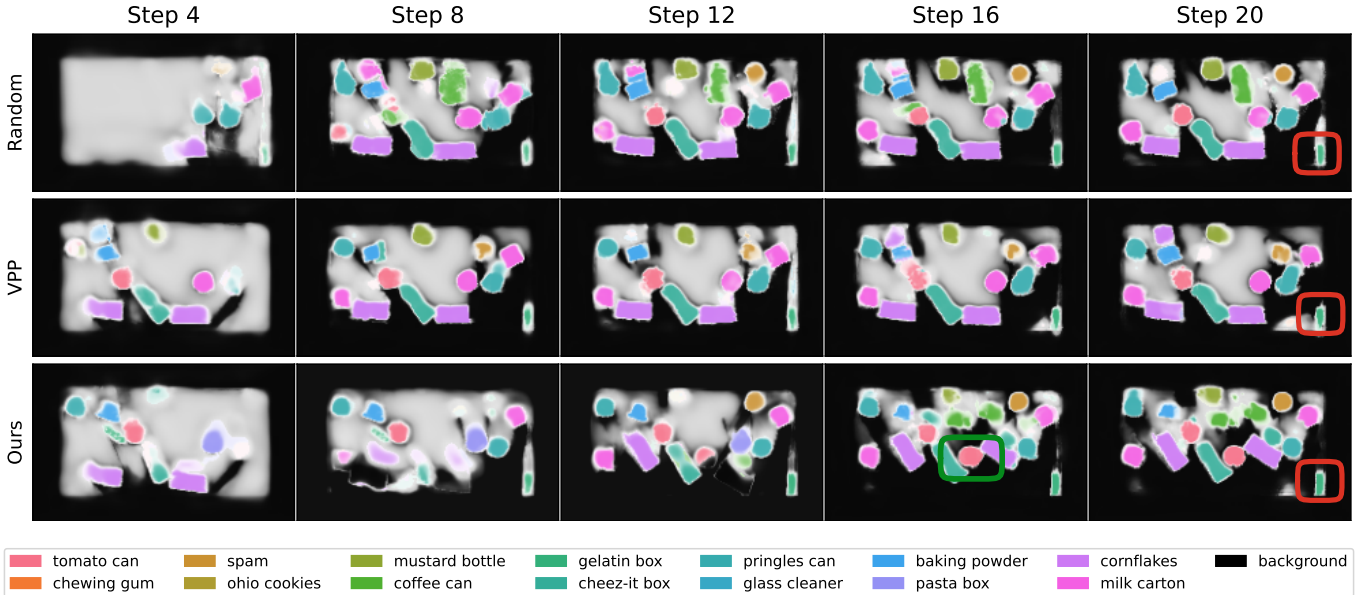


Fig. 7: Qualitative real-world experiment results. Note how VPP and Random baselines are unable to fully explore the environment due to its occlusions, while our method is able to better explore it via reasonable manipulations. In Step 16, ours, we highlight in green one of the scene objects revealed by our manipulations, while we highlight in red a persistent hallucination across all 3 methods, likely due to unreliable semantic segmentation and significant camera noise at the corner.

Computation times for our POMDP solver vary but take on the order of several seconds, due to the need for information gain calculations and belief propagation for many actions. Our current framework naively samples manipulation actions during action selection, and more intelligent action sampling could improve computational efficiency. This will be especially important when including additional manipulation actions, e.g., grasping.

There is currently a significant sim-to-real gap that could be addressed by fine-tuning on real data or performing domain randomization of the object dynamics during data collection in simulation to help improve real-world performance. Further, our maps are defined over dense voxel grids, which poses scalability challenges when applied to larger spaces. Moreover, the mapped region is a fixed volume and we assume prior knowledge about the fixed parts of the environment (e.g., shelf) for motion planning. These assumptions should be relaxed to address fully unstructured and unknown worlds. Finally, our maps use a closed-world semantic labeling, and extending belief propagation to open-world segmentation would be an interesting frontier to explore.

VII. CONCLUSION

This paper presented a POMDP approach to the manipulation-enhanced mapping problem in which the solver decides between changing a camera view and manipulating objects to map an area cluttered with objects. It relies on the novel Calibrated Neural-Accelerated Belief Update map-space belief propagation approach, which allows a unified treatment of both viewpoint change and manipulation actions. Using well-calibrated beliefs allows the POMDP solver to make decisions between different action types according to the best

informative outcome. Experimental results in both simulation and on a real robot show that our approach outperforms non-manipulating and heuristic manipulation baselines in terms of occupancy and semantic map accuracy. Overall, this work offers a promising new framework for robots navigating and manipulating real-world cluttered environments.

VIII. ACKNOWLEDGMENTS

This work used the NCSA Delta GPU cluster through allocation CIS240410 from the Advanced Cyberinfrastructure Coordination Ecosystem: Services & Support (ACCESS) program [2], which is supported by U.S. National Science Foundation grants #2138259, #2138286, #2138307, #2137603, and #2138296. This work has partly been supported by the European Commission under grant agreement numbers 964854 (RePAIR) and by the BMBF within the Robotics Institute Germany, grant #16ME0999. This work was also partially supported by NIFA/USDA Awards #2020-67021-32799 and #2021-67021-34418.

REFERENCES

- [1] Andreas Bircher, Mina Kamel, Kostas Alexis, Michael Burri, Philipp Oettershagen, Sammy Omari, Thomas Mantel, and Roland Siegwart. Three-dimensional coverage path planning via viewpoint resampling and tour optimization for aerial robots. *Autonomous Robots*, 40(6):1059–1078, 2016.
- [2] Timothy J. Boerner, Stephen Deems, Thomas R. Furlani, Shelley L. Knuth, and John Towns. Access: Advancing innovation: Nsf’s advanced cyberinfrastructure coordination ecosystem: Services & support. In *Practice and Experience in Advanced Research Computing 2023*:

Computing for the Common Good, PEARC '23, page 173–176, New York, NY, USA, 2023. Association for Computing Machinery. ISBN 9781450399852. doi: 10.1145/3569951.3597559. URL <https://doi.org/10.1145/3569951.3597559>.

[3] Jeannette Bohg, Karol Hausman, Bharath Sankaran, Oliver Brock, Danica Kragic, Stefan Schaal, and Gaurav S Sukhatme. Interactive perception: Leveraging action in perception and perception in action. *IEEE Transactions on Robotics*, 2017. doi: 10.1109/TRO.2017.2721939. URL <https://ieeexplore.ieee.org/document/8007233>.

[4] Berk Calli, Arjun Singh, Aaron Walsman, Siddhartha Srinivasa, Pieter Abbeel, and Aaron M Dollar. The YCB object and Model set: Towards common benchmarks for manipulation research. In *2015 International Conference on Advanced Robotics (ICAR)*, pages 510–517, 2015. doi: 10.1109/ICAR.2015.7251504.

[5] Berk Calli, Aaron Walsman, Arjun Singh, Siddhartha Srinivasa, Pieter Abbeel, and Aaron M Dollar. Benchmarking in manipulation research: The ycb object and model set and benchmarking protocols. *IEEE Robotics and Automation Magazine*, 2015.

[6] J Chase Kew, Brian Ichter, Maryam Bandari, Tsang-Wei Edward Lee, and Aleksandra Faust. Neural Collision Clearance Estimator for Batched Motion Planning. In Steven M LaValle, Ming Lin, Timo Ojala, Dylan Shell, and Jingjin Yu, editors, *Algorithmic Foundations of Robotics XIV*, pages 73–89, Cham, 2021. Springer International Publishing. ISBN 978-3-030-66723-8.

[7] Sachin Chitta, Ioan Sucan, and Steve Cousins. MoveIt! [ROS Topics]. *IEEE Robotics & Automation Magazine*, 19(1):18–19, 3 2012. ISSN 1070-9932. doi: 10.1109/MRA.2011.2181749. URL <http://ieeexplore.ieee.org/document/6174325>.

[8] Sanjiban Choudhury, Ashish Kapoor, Gireeja Ranade, and Debadatta Dey. Learning to gather information via imitation. In *2017 IEEE International Conference on Robotics and Automation (ICRA)*, pages 908–915, 2017. doi: 10.1109/ICRA.2017.7989112.

[9] Joao Marcos Correia Marques, Albert J Zhai, Shenlong Wang, and Kris Hauser. On the Overconfidence Problem in Semantic 3D Mapping. In *2024 IEEE International Conference on Robotics and Automation (ICRA)*, pages 11095–11102, 2024. doi: 10.1109/ICRA57147.2024.10611306.

[10] Erwin Coumans and Yunfei Bai. Pybullet, a python module for physics simulation for games, robotics and machine learning. <http://pybullet.org>, 2016–2021.

[11] Michael Danielczuk, Andrey Kurenkov, Ashwin Balakrishna, Matthew Matl, David Wang, Roberto Martín-Martín, Animesh Garg, Silvio Savarese, and Ken Goldberg. Mechanical search: Multi-step retrieval of a target object occluded by clutter. In *Proc. of the IEEE Intl. Conf. on Robotics & Automation (ICRA)*, 2019. doi: 10.1109/ICRA.2019.8794143. URL <https://ieeexplore.ieee.org/document/8794143>.

[12] Jeffrey Delmerico, Stefan Isler, Reza Sabzevari, and Davide Scaramuzza. A comparison of volumetric information gain metrics for active 3D object reconstruction. *Autonomous Robots*, 42(2):197–208, 2018. ISSN 1573-7527. doi: 10.1007/s10514-017-9634-0. URL <https://doi.org/10.1007/s10514-017-9634-0>.

[13] Nils Dengler, Sicong Pan, Vamsi Kalagaturu, Rohit Menon, Murad Dawood, and Maren Bennewitz. Viewpoint Push Planning for Mapping of Unknown Confined Spaces, 2023. URL <https://ieeexplore.ieee.org/document/10341809>.

[14] Georgios Georgakis, Bernadette Bucher, Karl Schmeckpeper, Siddharth Singh, and Kostas Daniilidis. Learning to Map for Active Semantic Goal Navigation. In *International Conference on Learning Representations*, 2022. doi: 10.48550/arXiv.2106.15648. URL <https://openreview.net/forum?id=swrMQtr6wN>.

[15] Sanchez Gildardo, , and Jean-Claude Latombe. A Single-Query Bi-Directional Probabilistic Roadmap Planner with Lazy Collision Checking. In Jarvis Raymond Austin, , and Alexander Zelinsky, editors, *Robotics Research*, pages 403–417, Berlin, Heidelberg, 2003. Springer Berlin Heidelberg. ISBN 978-3-540-36460-3.

[16] Danijar Hafner, Timothy Lillicrap, Jimmy Ba, and Mohammad Norouzi. Dream to Control: Learning Behaviors by Latent Imagination, 2020.

[17] K. Hauser. Robust contact generation for robot simulation with unstructured meshes. In *Proc. of the Intl. Symposium on Robotic Research (ISRR)*, 2013.

[18] Benjamin Hepp, Debadatta Dey, Sudipta N Sinha, Ashish Kapoor, Neel Joshi, and Otmar Hilliges. Learn-to-score: Efficient 3d scene exploration by predicting view utility. In *Proceedings of the European conference on computer vision (ECCV)*, pages 437–452, 2018. URL https://link.springer.com/chapter/10.1007/978-3-030-01267-0_27.

[19] H. Hu, S. Pan, L. Jin, M. Popović, and M. Bennewitz. Active implicit reconstruction using one-shot view planning. In *Proc. of the IEEE Intl. Conf. on Robotics & Automation (ICRA)*, 2024. doi: 10.1109/ICRA57147.2024.10611542. URL <https://ieeexplore.ieee.org/document/10611542>.

[20] Huang Huang, Marcus Dominguez-Kuhne, Vishal Satish, Michael Danielczuk, Kate Sanders, Jeffrey Ichnowski, Andrew Lee, Anelia Angelova, Vincent Vanhoucke, and Ken Goldberg. Mechanical search on shelves using lateral access x-ray. In *2021 IEEE/RSJ International Conference on Intelligent Robots and Systems (IROS)*, pages 2045–2052. IEEE, 2021. doi: 10.1109/IROS5116.2021.9636629. URL <https://ieeexplore.ieee.org/document/9636629>.

[21] Krishna Murthy Jatavallabhula, Alihusein Kuwajerwala, Qiao Gu, Mohd Osama, Tao Chen, Shuang Li, Ganesh Iyer, Soroush Saryazdi, Nikhil Keetha, Ayush Tewari, Joshua B Tenenbaum, Celso Miguel de Melo, Madhava

Krishna, Liam Paull, Florian Shkurti, and Antonio Torralba. ConceptFusion: Open-set Multimodal 3D Mapping, 2023.

[22] Leslie Pack Kaelbling, Michael L Littman, and Anthony R Cassandra. Planning and acting in partially observable stochastic domains. *Artificial Intelligence*, 101(1):99–134, 1998. ISSN 0004-3702. doi: [https://doi.org/10.1016/S0004-3702\(98\)00023-X](https://doi.org/10.1016/S0004-3702(98)00023-X). URL <https://www.sciencedirect.com/science/article/pii/S000437029800023X>.

[23] Seungyeon Kim, Young Hun Kim, Yonghyeon Lee, and Frank C Park. Leveraging 3d reconstruction for mechanical search on cluttered shelves. In *7th Annual Conference on Robot Learning*, 2023. URL <https://proceedings.mlr.press/v229/kim23a/kim23a.pdf>.

[24] Michael Krainin, Brian Curless, and Dieter Fox. Autonomous generation of complete 3d object models using next best view manipulation planning. In *2011 IEEE international conference on robotics and automation*, pages 5031–5037. IEEE, 2011.

[25] Andreas Krause, Ajit Singh, and Carlos Guestrin. Near-optimal sensor placements in Gaussian processes: Theory, efficient algorithms and empirical studies. *Journal of Machine Learning Research*, 9(2), 2008.

[26] Alex H Lang, Sourabh Vora, Holger Caesar, Lubing Zhou, Jiong Yang, and Oscar Beijbom. PointPillars: Fast Encoders for Object Detection From Point Clouds. In *Proceedings of the IEEE/CVF Conference on Computer Vision and Pattern Recognition (CVPR)*, 6 2019.

[27] Boyi Li, Kilian Q Weinberger, Serge Belongie, Vladlen Koltun, and René Ranftl. Language-driven Semantic Segmentation, 2022.

[28] Jue Kun Li, David Hsu, and Wee Sun Lee. Act to see and see to act: Pomdp planning for objects search in clutter. In *Proc. of the IEEE/RSJ Intl. Conf. on Intelligent Robots and Systems (IROS)*. IEEE, 2016. doi: 10.1109/IROS.2016.7759839. URL <https://ieeexplore.ieee.org/document/7759839>.

[29] Tingting Liang, Hongwei Xie, Kaicheng Yu, Zhongyu Xia, Zhiwei Lin, Yongtao Wang, Tao Tang, Bing Wang, and Zhi Tang. Bevfusion: A simple and robust lidar-camera fusion framework. In S. Koyejo, S. Mohamed, A. Agarwal, D. Belgrave, K. Cho, and A. Oh, editors, *Advances in Neural Information Processing Systems*, volume 35, pages 10421–10434. Curran Associates, Inc., 2022. URL https://proceedings.neurips.cc/paper_files/paper/2022/file/43d2b7fbee8431f7cef0d0afed51c691-Paper-Conference.pdf.

[30] Zhijian Liu, Haotian Tang, Alexander Amini, Xingyu Yang, Huiyi Mao, Daniela Rus, and Song Han. Bevfusion: Multi-task multi-sensor fusion with unified bird’s-eye view representation. In *Proc. of the IEEE Intl. Conf. on Robotics & Automation (ICRA)*, 2023. doi: 10.1109/ICRA48891.2023.10160968. URL <https://ieeexplore.ieee.org/document/10160968>.

[31] Joao Marcos Correia Marques, Albert J Zhai, Shenlong Wang, and Kris Hauser. On the overconfidence problem in semantic 3d mapping. In *Proc. of the IEEE Intl. Conf. on Robotics & Automation (ICRA)*. IEEE, 2024.

[32] Riccardo Monica and Jacopo Aleotti. Contour-based next-best view planning from point cloud segmentation of unknown objects. *Autonomous Robots*, 42(2):443–458, 2018. URL <https://link.springer.com/article/10.1007/s10514-017-9618-0>.

[33] Adam Paszke, Sam Gross, Francisco Massa, Adam Lerer, James Bradbury, Gregory Chanan, Trevor Killeen, Zeming Lin, Natalia Gimelshein, Luca Antiga, Alban Desmaison, Andreas Kopf, Edward Yang, Zachary DeVito, Martin Raison, Alykhan Tejani, Sasank Chilamkurthy, Benoit Steiner, Lu Fang, Junjie Bai, and Soumith Chintala. PyTorch: An Imperative Style, High-Performance Deep Learning Library. In H Wallach, H Larochelle, A Beygelzimer, F d’Alché Buc, E Fox, and R Garnett, editors, *Advances in Neural Information Processing Systems 32*, pages 8024–8035. Curran Associates, Inc., 2019. URL <http://papers.neurips.cc/paper/9015-pytorch-an-imperative-style-high-performance-deep-learning-library.pdf>.

[34] Thomas Pitcher, Julian Förster, and Jen Jen Chung. Reinforcement learning for active search and grasp in clutter. In *Proc. of the IEEE/RSJ Intl. Conf. on Intelligent Robots and Systems (IROS)*. IEEE, 2024. doi: 10.1109/IROS58592.2024.10801366. URL <https://ieeexplore.ieee.org/document/10801366>.

[35] Alec Radford, Jong Wook Kim, Chris Hallacy, Aditya Ramesh, Gabriel Goh, Sandhini Agarwal, Girish Sastry, Amanda Askell, Pamela Mishkin, Jack Clark, Gretchen Krueger, and Ilya Sutskever. Learning Transferable Visual Models From Natural Language Supervision, 2021.

[36] Nikhila Ravi, Valentin Gabeur, Yuan-Ting Hu, Ronghang Hu, Chaitanya Ryali, Tengyu Ma, Haitham Khedr, Roman Rädle, Chloe Rolland, Laura Gustafson, et al. Sam 2: Segment anything in images and videos. *arXiv preprint arXiv:2408.00714*, 2024.

[37] Dhruv Saxena and Maxim Likhachev. Planning for manipulation among movable objects: Deciding which objects go where, in what order, and how. In *Proc. of the Int. Conf. on Automated Planning and Scheduling (ICAPS)*, 2023.

[38] Dhruv Mauria Saxena and Maxim Likhachev. Improved m4m: Faster and richer planning for manipulation among movable objects in cluttered 3d workspaces. In *Proc. of the IEEE Intl. Conf. on Robotics & Automation (ICRA)*. IEEE, 2024. doi: 10.1109/ICRA57147.2024.10611234. URL <https://ieeexplore.ieee.org/document/10611234>.

[39] Murat Sensoy, Lance Kaplan, and Melih Kandemir. Evidential Deep Learning to Quantify Classification Uncertainty. In S Bengio, H Wallach, H Larochelle, K Grauman, N Cesa-Bianchi, and R Garnett, editors, *Advances in Neural Information Processing Systems*, volume 31. Curran Associates, Inc., 2018. URL <https://proceedings>.

neurips.cc/paper_files/paper/2018/file/a981f2b708044d6fb4a71a1463242520-Paper.pdf.

- [40] Satvik Sharma, Kaushik Shivakumar, Huang Huang, Lawrence Yunliang Chen, Ryan Hoque, brian ichter, and Ken Goldberg. Open-World Semantic Mechanical Search with Large Vision and Language Models. In *7th Annual Conference on Robot Learning*, 2023. URL <https://openreview.net/forum?id=vsEWu6mMUhB>.
- [41] Satvik Sharma, Kaushik Shivakumar, Huang Huang, Ryan Hoque, Alishba Imran, Brian Ichter, and Ken Goldberg. From Occlusion to Insight: Object Search in Semantic Shelves using Large Language Models. *arXiv preprint arXiv:2302.12915*, 2023. doi: 10.48550/ARXIV.2302.12915. URL <https://arxiv.org/pdf/2302.12915>.
- [42] Mike Stilman, Jan-Ullrich Schamburek, James Kuffner, and Tamim Asfour. Manipulation planning among movable obstacles. In *Proc. of the IEEE Intl. Conf. on Robotics & Automation (ICRA)*. IEEE, 2007.
- [43] Sebastian Thrun, Wolfram Burgard, and Dieter Fox. Probabilistic robotics. 2005. *Massachusetts Institute of Technology, USA*, 2005.
- [44] Dennis Ulmer, Christian Hardmeier, and Jes Frellsen. Prior and Posterior Networks: A Survey on Evidential Deep Learning Methods For Uncertainty Estimation. *PMLR*, 2023.
- [45] Dani Valevski, Yaniv Leviathan, Moab Arar, and Shlomi Fruchter. Diffusion models are real-time game engines, 2024. URL <https://arxiv.org/abs/2408.14837>.
- [46] Yuchen Xiao, Sammie Katt, Andreas ten Pas, Shengjian Chen, and Christopher Amato. Online planning for target object search in clutter under partial observability. In *Proc. of the IEEE Intl. Conf. on Robotics & Automation (ICRA)*. IEEE, 2019. doi: 10.1109/ICRA.2019.8793494. URL <https://ieeexplore.ieee.org/document/8793494>.
- [47] Sherry Yang, Yilun Du, Seyed Kamyar Seyed Ghasemipour, Jonathan Tompson, Leslie Pack Kaelbling, Dale Schuurmans, and Pieter Abbeel. Learning interactive real-world simulators. In *The Twelfth International Conference on Learning Representations*, 2024. URL <https://openreview.net/forum?id=sFyTZEqmUY>.
- [48] Rui Zeng, Yuhui Wen, Wang Zhao, and Yong-Jin Liu. View planning in robot active vision: A survey of systems, algorithms, and applications. *Computational Visual Media*, 2020. URL <https://link.springer.com/article/10.1007/s41095-020-0179-3>.
- [49] Albert J Zhai and Shenlong Wang. PEANUT: Predicting and Navigating to Unseen Targets. In *Proceedings of the IEEE/CVF International Conference on Computer Vision (ICCV)*, pages 10926–10935, 10 2023. doi: 10.1109/ICCV51070.2023.01003. URL <https://ieeexplore.ieee.org/document/10378364>.

APPENDIX

A. Dataset Generation Details

The simulation environment used for data generation and simulation testing is PyBullet [10] (Fig. 8). The object arrangements for the CNABU training datasets were created according to the following procedure: First, we sample the desired occupancy fraction of the shelf floor plan - which we set to be between 30 and 45%. We define two parameters for each object class: its affinity to other classes and its radius of influence. Classes within an object’s affinity class and radius of influence have their probability of appearance increased. Further, we define a regularity parameter, ρ for the generation, from 0 to 1. When this parameter is zero, there is no enforced alignment in the shelf and when it is one, there is a higher probability for objects to be placed directly in line with the centroid of previously placed objects, emulating more orderly arrangements by increasing the probability of sampling areas directly in front or behind already placed objects.

We begin sampling by placing a fine grid over the floor space of the scene. Then, until the desired shelf occupancy is reached (or a total number of iterations is reached), we sample a point in this grid that is not yet occupied by another object - taking into consideration the altered probabilities of occupancy by ρ . Through the use of Minkowski differences between the object shapes and the free space, we determine the placeable area for the centroid of each object class within the current arrangement and, for each object that is placeable in the selected point, we compute its sampling probability conditioned on the affinities of the objects whose area of influence contains the sampled point. We then sample an object class according to that distribution and randomly sample an angle for the object, between 0° and 180° and place the object in that orientation. To stimulate the presence of occlusions, we set the base probability of larger objects to be slightly higher - and set large objects to have affinity for smaller objects. For dataset generation, we leave ρ at 0. The ground truth map for each scenario is collected by removing the top shelf, taking a series of dense top-down images of the scene and mapping them with traditional metric-semantic grid mapping [31]. For the pushing dataset, the scenario sampling is identical, except we also sample a random push following Sec. IV-E.

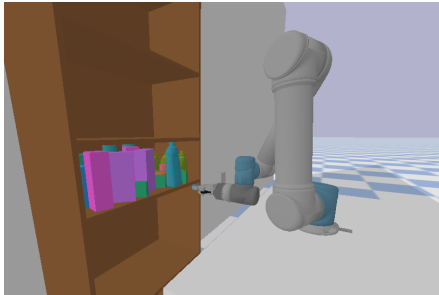


Fig. 8: Simulation environment configuration example of different YCB objects in a confined shelf scenario. The UR5 is equipped with a Robotiq parallel-jaw gripper

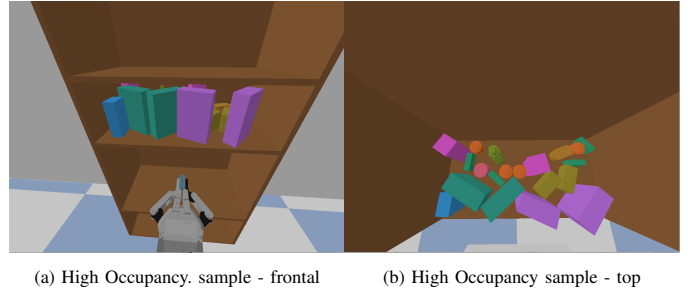


Fig. 9: Frontal and (privileged) top-down views of a scene from the highly occluded set



Fig. 10: Frontal and (privileged) top-down views of a scene from the Slightly Occluded set (right).

Figures 9 and 10 show example scenes from the High Occupancy and Low Occupancy sets. Note how both scenes have occluded objects which are hard to see from any viewpoint - but the HOS scene has more occluded objects - and a much more challenging manipulation environment to uncover the occlusions.

B. CNABU Implementation Details

We used network architectures similar to Georgakis et al. [14], with the exception that the output heads are set to be posterior networks. Our network structure can be seen in Fig. 3. The occupancy head in both architectures is a 1×1 convolution, while the differences head in the push prediction network is a series of Convolutional + ReLU + BatchNorm layers followed by a 1×1 convolution. The semantic head is similar to the differences head. Their losses and training are described in Sec. IV-G. We used BEVFusion’s [30] approach of feeding the voxel heights as additional channels to 2D Res-UNets [29, 26]. For processing the voxel grids as inputs.

The networks are trained using backpropagation in PyTorch [33], with grid search-optimized learning rates and ADAM optimizer, as well as early stopping based on the validation loss. The dataset for training σ_o consists of 30.000 randomly sampled scenes, while the dataset for training σ_m consists of 11.700 pushes. Both datasets were split into train, validation and test splits at a ratio of 0.8:0.1:0.1. Dataset generation details are discussed in Sec. A of the appendix. For added robustness in real-world scenarios, we augment the simulation data with salt-and-pepper noise, random rotations and translations and add Gaussian noise to the depth images.

TABLE II: Summary of features of all considered baselines

Baseline Name	Use σ_o	VPP	Use σ_m	Push	Action Selection
Ours	yes	yes	yes	yes	Sec. IV-D
Ours - Pushing	yes	yes	no	no	no
Random + Viewpoint CNABU	yes	no	no	no	no
Random	no	no	no	no	no
Interval Random Pushing	yes	yes	yes	yes	Random every 5 steps
Interval Pushing No Push CNABU	yes	yes	no	yes	Random every 5 Steps
Random View Interval Random Pushing	yes	no	no	yes	Random every 5 steps
Saturation Pushing	yes	yes	yes	yes	Random upon VPP saturation
Dengler et al. [13]	no	yes, RL-Based	no	yes	Push classifier network upon saturation

C. Prompts used for Semantic Segmentation

To perform semantic segmentation of the SAM2 masks, we use the embeddings of the following text prompts to classify the segments:

- tomato can - "tomato or kidney beans round tin can"
- chewing gum - "small round chewing gum box"
- spam: "potted meat tin can, spam"
- ohio cookies - "ohio cookie box in purple cardboard carton cookies",
- mustard bottle - "yellow frenchy's mustard bottle",
- coffee can - "maxwell house coffee can with blue wrapper",
- gelatin box - "light pink gelatin box",
- cheez-it box - "cheezeit cracker box in dark red color",
- pringles can - "pringles chips tube cylinder red or green", "in red color or green color bottles with transparent lid",
- glass cleaner - "glass cleaner spray plastic bottle",
- baking powder - "koop mans baking powder box",
- pasta box - "Big blue carton of pasta collezione"
- Cornflakes - "kölln schoko cronflakes in yellow brown cardboard box cereal"
- milk carton - "milk box tetrapak blue label voll milch",
- shelf - "wooden shelf board", "cream colored wooden shelf of light cream color"
- black - "just black"

In this case, both "shelf" and "black" were used as synonymous of the background class, capturing different failure cases of SAM2 segmentation.

D. Summary of baseline features

We summarize the considered baselines in Tab. II to facilitate comparing their features.